

## HIGH-CADENCE OBSERVATIONS OF AN IMPULSIVE FLARE

HAIMIN WANG, JIONG QIU, CARSTEN DENKER, TOM SPIROCK, HANGJUN CHEN, AND PHILIP R. GOODE

Big Bear Solar Observatory, New Jersey Institute of Technology, 40386 North Shore Lane, Big Bear City, CA 92314-9672; haimin@solar.njit.edu

Received 2000 April 11; accepted 2000 June 7

### ABSTRACT

We analyzed high-cadence observations of a C5.7 flare on 1999 August 23 at Big Bear Solar Observatory (BBSO). The observing wavelength was  $1.3 \text{ \AA}$  in the blue wing of  $H\alpha$ , with a cadence of 0.033 s. In addition, the hard X-ray's time profile obtained by the Burst And Transient Source Experiment (BATSE) and BBSO high-resolution magnetograms was compared with our  $H\alpha$  observations to understand in detail the particle precipitation in this event. The important results are as follows:

1. In  $H\alpha - 1.3 \text{ \AA}$ , three flare kernels were observed in the early phase of the flare. The flare started in a nonmagnetic area at the magnetic neutral line. This suggests to us that the top of a low-lying loop is the initial energy release site, while the other two kernels are the footpoints of another overlying flare loop, formed after the magnetic reconnection.

2. We analyzed the temporal behavior of the three flare kernels in the impulsive phase when hard X-ray (HXR) emission was significant. We found that during a 7 s period, the  $H\alpha - 1.3 \text{ \AA}$  brightenings at one of the footpoints showed a very good temporal correlation with the HXR flux variation. Therefore, from the spatially resolved  $H\alpha$  off-band observations, we identified this flare kernel as the source of HXR emission.

3. From the footpoint which exhibits the best correlation with HXR emission, the  $H\alpha - 1.3 \text{ \AA}$  emission shows high-frequency fluctuations on a timescale of a few tenths of a second. The amplitude of the fluctuations is more than 3 times the noise. Such fluctuations are not evident in the other flare kernels which also do not show good correlation with HXR emission. For this reason, we suggest that the observed high-frequency fluctuations may be signatures of temporal fine structure related to the HXR elementary bursts.

*Subject headings:* Sun: activity — Sun: flares — Sun: magnetic fields

### 1. INTRODUCTION

High-cadence X-ray and microwave observations exhibit a subsecond temporal fine structure in solar flares, called elementary flare bursts (see Sturrock 1989 for review). They are attributed to the fine structure in coronal magnetic fields and related to the aggregation of photospheric magnetic fields into small-scale magnetic elements. From a sample of nearly 3000 HXR solar flares as observed with the HXR burst spectrometer on the *Solar Maximum Mission* (SMM), Kiplinger et al. (1983) found that a portion of the events has a subsecond temporal structure. More recent HXR observations from BATSE on board the *Compton Gamma-Ray Observatory* (CGRO) provide a much improved sensitivity and energy resolution, and a temporal resolution down to 64 ms. Aschwanden et al. (1996) used the subsecond temporal structure to study the scales of magnetic loops in flares by applying the time-of-flight method. However, the above observations are only moderately resolved in time, and they lack spatial resolution and information about the corresponding magnetic structure.

Impulsive hard X-ray emission in the early phase of a flare is generally regarded as a result of collisional degradation of nonthermal electrons in the dense chromosphere (“thick-target”) by nonthermal bremsstrahlung (Brown 1971; Emslie 1978). The heating and ionization of the chromosphere by nonthermal electrons can produce optical (e.g.,  $H\alpha$ ) emission nearly simultaneously with hard X-ray bursts (Canfield, Gunkler, & Ricchiazzi 1984; Fisher, Canfield, & McClymont 1985; Canfield & Gayley 1987; Hawley & Fisher 1994; Abbett & Hawley 1999). Specifically, the emission in the wing of the  $H\alpha$  line may be produced via

Stark broadening by electrons moving down to the deep chromosphere (e.g., Svestka 1976). In more detail, the emission is due to nonthermal ionization by the fast electrons down to the deep chromosphere. The ionization could this way increase the electron number density in the deep chromosphere by an order of magnitude, and the microelectric field thus produced can cause Stark effect—the split of atomic levels. Several authors have actually calculated the electron number density and line profiles (Canfield, Gunkler, & Ricchiazzi 1984; Fang, Henoux, & Gan 1993).

Spatially resolved observations in the line wings of  $H\alpha$  can be used to track down the precipitating sites of the nonthermal electrons which also produce HXR emission (Canfield & Gayley 1987; Wulser & Marti 1989; de La Beaujardiere, Kiplinger, & Canfield 1992). There have been some efforts to observe temporal fine structures during the impulsive phase with moderate spatial resolution. High-cadence  $H\alpha$  observations were carried out with a system developed by Kiplinger (Kiplinger, Dennis, & Orwig 1989; Neidig et al. 1993) with a time cadence of 0.5 s. Kaempfer & Magun (1983) studied the evolution of  $H\alpha$  flares with a 1.4 s cadence. These studies could identify some flare footpoints as sites of precipitation, from which the optical emissions exhibited no, or very short, delay (1–2 s) with respect to the HXR bursts and microwave emission. However, the temporal resolution of these observations is still not sufficient to monitor the often reported subsecond variations of “elementary bursts,” and the moderate spatial resolution is not sufficient to reveal the intrinsic details of the emission sources.

A new fast frame rate (30 fps) CCD camera recently

installed at BBSO enables us to study solar flares with an order of magnitude shorter temporal resolution. Magnetograms of moderate temporal resolution (1 minute) and spatial resolution (approximately  $1''$ ) provide important context data. Observing under BBSO's excellent seeing conditions (Goode et al. 2000), we expect to obtain more information on temporal and spatial fine structures of impulsive flares. In the near future, we expect to combine our observations with the High Energy Solar Spectroscopic Imager (HESSI) mission (Lin et al. 1998) for even more detailed investigations on fine structures of solar flares.

## 2. OBSERVATIONS AND DATA REDUCTION

The *GOES* C5.7 flare occurred at 18:09 UT on 1999 August 23 in active region NOAA 8673. It was also observed by BATSE on board *CGRO*. Unfortunately, because of the low flux of this flare, BATSE did not trigger its high-cadence mode. The cadence of the available continuum data is 1.024 s.

The observations at BBSO completely cover this flare. High-cadence  $H\alpha$  observations in the far blue wing are the key data set for this study. We used a  $1024 \times 1024$  pixel, 12-bit frame transfer CCD camera manufactured by Silicon Mountain Design (SMD). The SMD 1M15 camera is binned to  $512 \times 512$  pixels to increase the signal-to-noise ratio and the frame rate from 15 fps to 30 fps. Such high frame rate is achieved at the cost of continuous coverage which results in an interruption of 15 s for every 200 frames, or 7 s of data. The exposure time of each individual frame is 8 ms. The image scale is about  $0''.39 \text{ pixel}^{-1}$ . We selected the observing wavelength by using a Zeiss filter with a bandpass of  $0.25 \text{ \AA}$ . The filter is tuned to  $1.3 \text{ \AA}$  in the blue wing of  $H\alpha$  to study the impulsive behavior of flares, since the center line contains thermal contamination, and the red wing contains the component of chromospheric condensation (Canfield & Gayley 1987).

Supplementary full-disk  $H\alpha$  center-line observations are obtained routinely every day with a cadence of 30 s to 1 minute and a spatial resolution of about  $2''$  (Denker et al. 1999). Magnetic fields in the active region are observed with the videomagnetograph system (Varsik 1995). Its image scale is  $0''.5 \text{ pixel}^{-1}$ , and the cadence is 1 minute. Only line-of-sight magnetic fields were measured on that day. All the data sets are carefully aligned with standard methods developed by the BBSO group. The accuracy of alignment is usually better than  $1''$ .

## 3. RESULTS

### 3.1. General View of the Flare

In Figure 1, the integrated light curves at different wavelengths are presented. The flare exhibits a typical impulsive phase defined by the impulsive HXR emission showing both fast rise and fast decay. The 25–50 keV HXR flux is detected by the most sunward detector of BATSE. The HXR emission lasts for about 1 minute and consists of several spikes each in the order of less than 10 s. We believe that these HXR temporal structures are due to continuous acceleration of nonthermal electrons. The main phase is defined by the gradual SXR 1–8  $\text{\AA}$  (*plus signs*) and  $H\alpha$  line center (*dotted curve*) emission which peak a few minutes after the HXR emission. The rise and decay rates of the  $H\alpha - 1.3 \text{ \AA}$  emission (*dashed line*) are between the rates for HXR and SXR as anticipated from the calculation by Canfield & Gayley (1987).

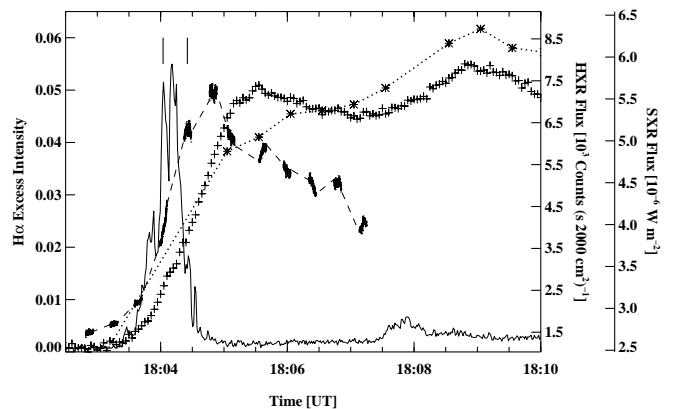


FIG. 1.—Time profiles of *GOES* soft X-ray (+), BATSE hard X-ray (solid line),  $H\alpha$  line center (dotted line), and  $H\alpha - 1.3 \text{ \AA}$  (dashed line) emissions of the 1999 August 23 flare. The  $H\alpha$  light curves indicate the excess emission, i.e., the flare intensity with the quiet region intensity subtracted and then normalized to the quiet region intensity. The two vertical bars in the plot indicate the two time intervals of the  $H\alpha - 1.3 \text{ \AA}$  emission analyzed in the paper and plotted in Figs. 5 and 6.

Figure 2 demonstrates the morphology of the flare. The top six panels show the sequence of  $H\alpha - 1.3 \text{ \AA}$  images during the impulsive phase, and the bottom six panels show  $H\alpha$  line center images throughout the flare evolution. The line center images were from full-disk observations, so the resolution appears to be lower. The flare starts close to a filament, and at 18:02:49 UT, a section of the dark filament appears in the blue band image, indicating a partial eruption of the filament. In the  $H\alpha$  blue wing, an early brightening (K2) appears at this location in less than 1 minute. Two other bright kernels (K1 and K3) appear at about 18:03:59 UT, 1 minute after the brightening of the center patch. From the center-line images in the later period, the flare brightening is visible in a much more extended area and evolves into a more complicated structure. However, we can see that the emission at K3 disappears earlier than at the other sites.

It is important to understand the magnetic structure of the flare. Figure 3 shows the evolution of the flare superposed on the magnetogram. The intensity of the flare at  $H\alpha - 1.3 \text{ \AA}$  is presented in contour maps, covering the period 18:02:51 UT–18:07:16 UT. All the images are background subtracted, i.e., subtracted by the image at 18:02:00 UT. The magnetogram, obtained at 18:02 UT, is presented as a gray-scale which serves as the background in all the panels. The initial brightening K2 at 18:03 UT is not on any magnetic element. Instead, it appears between two magnetic elements of opposite polarity. This is somehow surprising, since the  $H\alpha$  far wing should show sites of particle precipitation, which are usually located at the footpoints of the magnetic loops. K1 and K3, on the other hand, are cospatial with magnetic elements. This may be due to magnetic reconnection between two loops,  $K1^- - K2^+$  and  $K2^- - K3^+$ , as illustrated by the sketch in Figure 9. The loop  $K1^- - K2^+$  connects the negative polarity at K1 and the positive polarity at K2, and the loop  $K2^- - K3^+$  connects the negative polarity at K2 and positive polarity at K3. After reconnection, the newly formed low-lying loop,  $K2^+ - K2^-$ , was very close to the chromosphere, and appears as the initial brightening of the flare. Since the two footpoints  $K2^+$  and  $K2^-$  were very close, the emission at K2 cannot be spatially resolved.

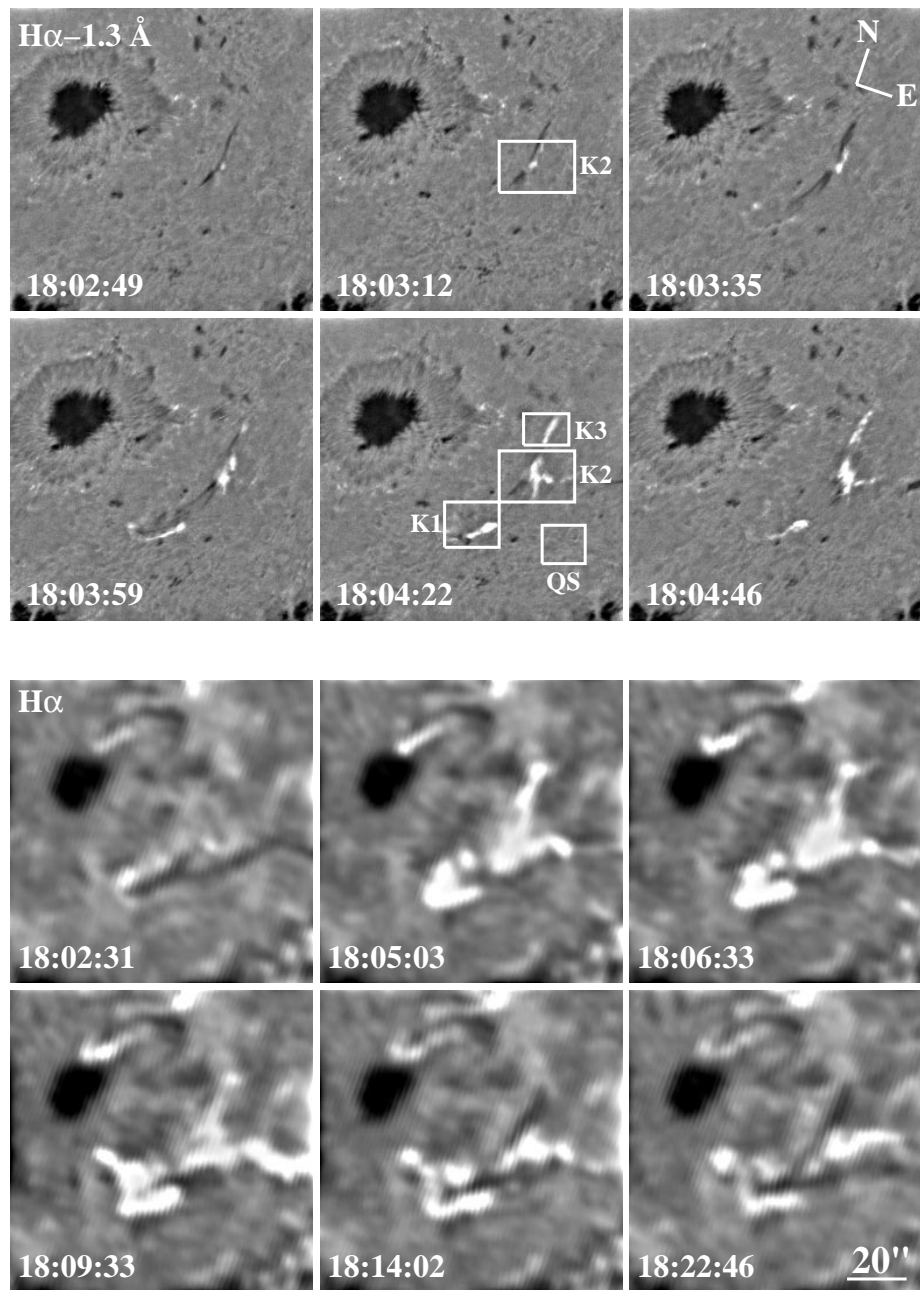


FIG. 2.—Time sequence of  $H\alpha - 1.3 \text{ \AA}$  (top six panels) and  $H\alpha$  line center (bottom six panels) images showing the evolution of the flare. The white boxes in the figure indicate the regions where we obtain the  $H\alpha - 1.3 \text{ \AA}$  light curves at the three flare kernels and the quiet-Sun region.

In the following sections, we do not distinguish whether the  $H\alpha - 1.3 \text{ \AA}$  emission was from the footpoint or from the loop top, but refer to the bright patches as “flare kernels.”

### 3.2. Evolution of Flare Kernels

To further analyze the evolution of the spatially resolved flare emission, we obtain the light curves of the individual flare kernels. We defined three regions covering the three flare kernels, as indicated by the white boxes in Figure 2. For each box, we computed the mean of the flare intensity subtracting the quiet-Sun region intensity and then normalizing to the quiet-Sun region intensity. These light curves indicate the temporal evolution of the excess flare emission at  $H\alpha$  line.

Figure 4 shows the light curves at the three flare kernels. The three kernels apparently exhibit different temporal profiles. The emissions in K1 and K3 both demonstrate fast rise, and the decay phase consists of two episodes, the fast decay followed by a slow decay, similar to the findings of Kaempfer & Magun (1983).

It is interesting that K2 also shows two distinct episodes in its evolution. Up to 18:04:30 UT, the light curve shows more similarity to the HXR bursts, though  $H\alpha$  data at the HXR maximum are missing, and there is enhanced emission even before the HXR starts to rise. After the impulsive phase, the  $H\alpha$  emission displays a gradual behavior, and the temporal evolution shows more similarity to the SXR emission. The temporal behavior of the spatially resolved flare

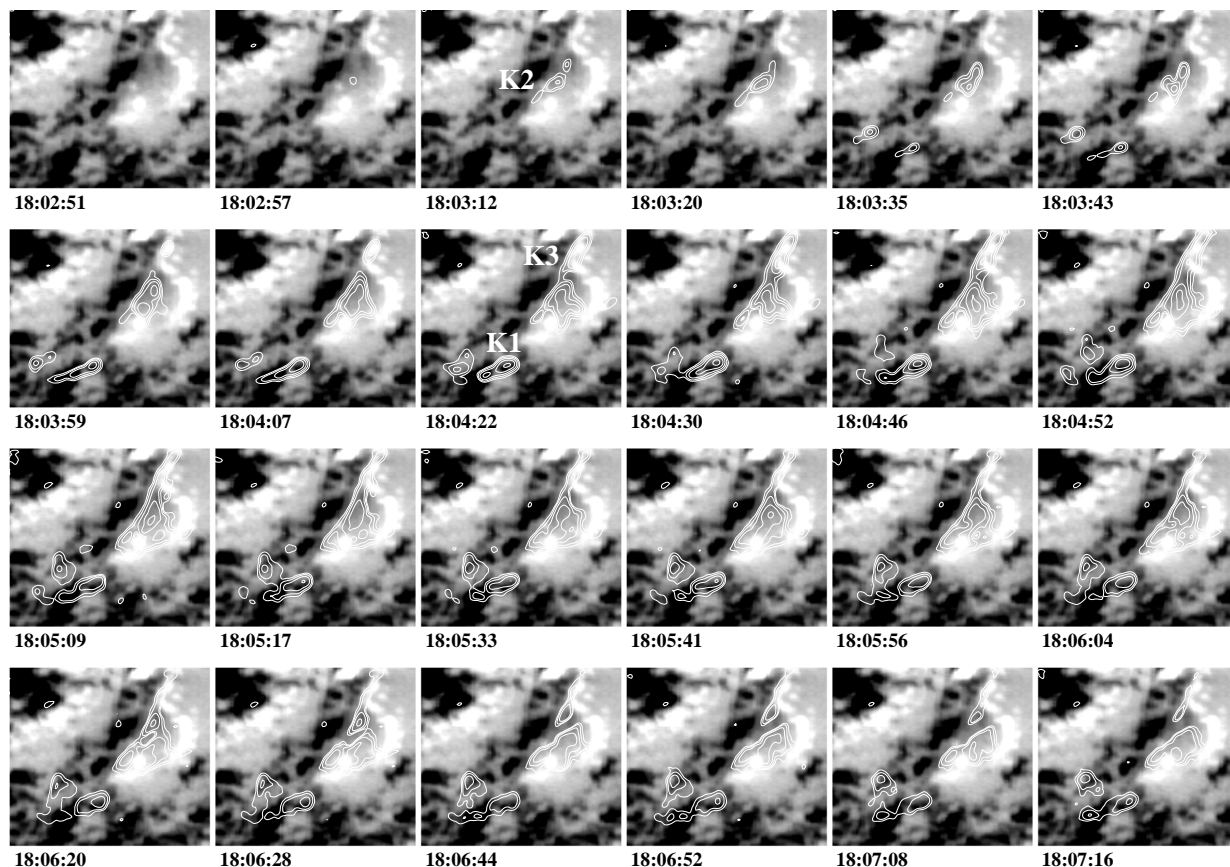


FIG. 3.—Time sequence of  $H\alpha-1.3 \text{ \AA}$  flare emission as shown by contours; the contour levels are 0.05, 0.1, 0.2, 0.4, 0.8 of the maximum of the emission. The background is the magnetogram obtained right before the flare.

kernels confirms the scenario suggested above, that K2 is the site where two magnetic loops reconnect. The initial energy release occurs at K2, and soon the accelerated electrons precipitate along the reconnecting loops to produce the HXR emission and the impulsive  $H\alpha$  blue wing emission.

### 3.3. Temporal Correlation with HXR

The unprecedented high-cadence observations offer a unique opportunity to investigate the possible correlation between the HXR bursts and deep chromospheric emission on a fine timescale. Specifically, three of the  $H\alpha-1.3 \text{ \AA}$  data sets are obtained during the impulsive phase when there is significant HXR emission.

1. *Time interval 18:03:35–18:03:41 UT*—During this period, the HXR emission rises monotonically, and so are the emissions at K1 and K2. This suggests that the chromosphere at these two sites, probably as conjugate footpoints of loop  $K1^- - K2^+$ , begins to be heated by nonthermal electrons. But the HXR photon counts during this period are still too low for any detailed investigation.

2. *Time interval 18:03:59–18:04:06 UT*—Figure 5 shows the temporal evolution of the  $H\alpha-1.3 \text{ \AA}$  intensities for the three kernels and a corresponding 10-point smoothed curves, as well as the HXR flux (*thick line*) from the most sunward detector of BATSE. During this period, the HXR emission shows a peak, while all three  $H\alpha$  kernels exhibit a monotonic rise. Because of the data gap at the  $H\alpha-1.3 \text{ \AA}$ , we cannot tell the exact time lag between the

HXR maximum and  $H\alpha-1.3 \text{ \AA}$  maximum, but the delay is at least 2–3 s. The temporal correlation between any of the two kernels is strong (greater than 80%), suggesting simultaneous chromospheric heating at all three sites.

3. *Time interval 18:04:22–18:04:29 UT*—In this period, HXR shows two spikes, which are covered by the  $H\alpha$  blue wing observations. This time interval gives the best opportunity to investigate the temporal correlation between HXR and  $H\alpha-1.3 \text{ \AA}$  emission. Figure 6 illustrates the  $H\alpha-1.3 \text{ \AA}$  intensities at the three kernels and the hard X-ray flux in this time interval. It is obvious that in K2, there is no correlation between X-ray and  $H\alpha$  emission. K3 shows some degree of linear correlation (54%) between HXR and  $H\alpha$  emission, while K1 has the best correlation (92%) within the HXR time resolution. It is evident that continuous electron acceleration is present during this period, and the HXR source could be located at K1 with some contribution from K3. This also suggests that in this event during the late impulsive phase, continuous electron precipitation occurs at the conjugate footpoints of the newly formed  $K1^- - K3^+$  loop.

The difference in the time profiles of the  $H\alpha$  kernels at different time intervals will be discussed in § 4.

### 3.4. High-Frequency Fluctuation in the Flare Kernels

During the C5.7 flare event, the BATSE HXR detector was working at rather low cadence. However, the  $H\alpha$  blue wing emission, especially during times of strong temporal correlation with HXR bursts, can be used as a proxy for

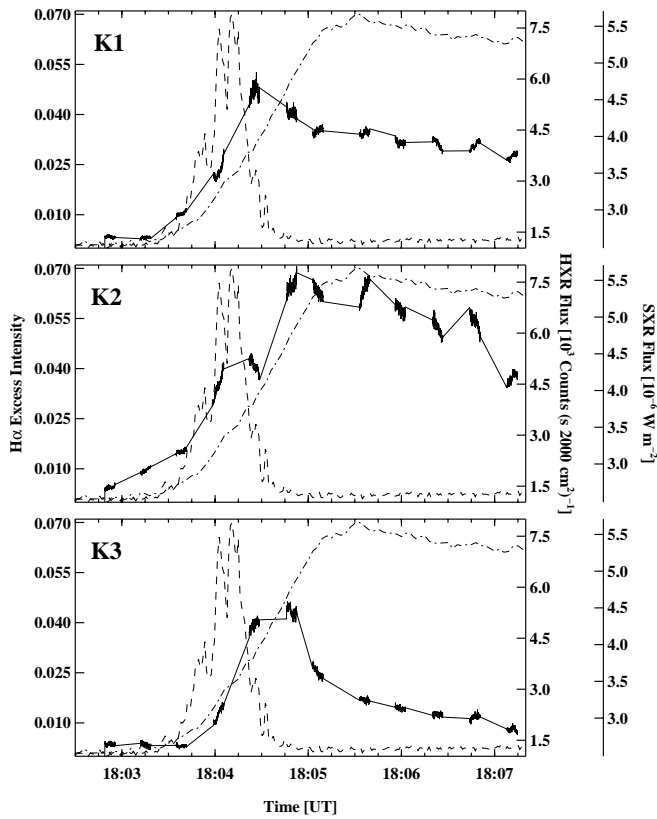


FIG. 4.—Time profiles of the flare emission in  $H\alpha-1.3 \text{ \AA}$  at three flare kernels (solid line) compared with BATSE hard X-ray emission (dashed line) and GOES soft X-ray  $1-8 \text{ \AA}$  emission (dot-dashed line).

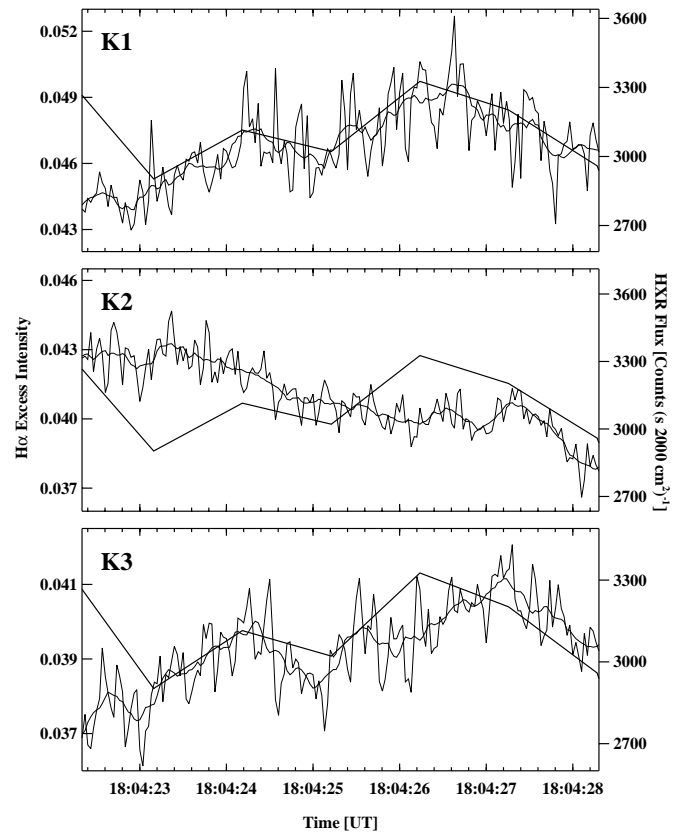


FIG. 6.—Comparison of  $H\alpha-1.3 \text{ \AA}$  intensity (thin lines) and hard X-ray flux (thick lines) for three flare kernels during the time interval 18:04:22–18:04:29 UT. For the  $H\alpha$  emission, both the raw data and a 10-point smoothed curve are plotted.

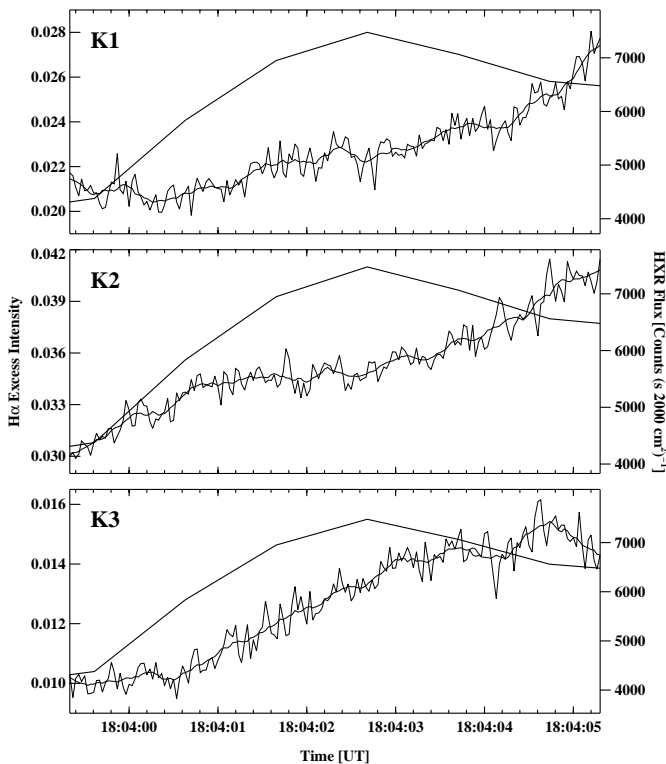


FIG. 5.—Comparison of  $H\alpha-1.3 \text{ \AA}$  intensity (thin lines) and hard X-ray flux (thick lines) for three flare kernels during the time interval 18:03:59–18:04:06 UT. For the  $H\alpha$  emission, both the raw data and a 10-point smoothed curve are plotted.

electron beam heating to examine high-frequency fluctuations. We first examine the fluctuations due to seeing and the temporal variations of the sky brightness. The seeing-induced fluctuations are determined from the contrast variations of a quiet-Sun region. They are in the order of only 0.05%. The variations in the sky brightness are determined from the light curve of the quiet-Sun region, and they are about 0.06%. Therefore, the fluctuations due to both seeing variations and the change of the sky brightness are negligible in the following analysis. In Figure 6, we note some larger fluctuations at K1 than at K2 and K3. In the top three panels of Figure 7, we show the same light curves as Figure 6 but with the low-frequency component subtracted. The amplitude of the fluctuations at K1 is greater than at K2 and K3, and the standard deviation of the high-frequency components at K1 is about twice of that at K2 and K3.

To estimate the frequency of the fast variations, we compute the temporal power spectrum of the H $\alpha$  light curves. We use a Hanning high-pass filter with a cutoff of 1 s to remove slow variations. Figure 8 illustrates the power spectra of the  $H\alpha-1.3 \text{ \AA}$  residual intensity at K1, K2, and K3. It evidently exhibits fast variations at K1 with a dominant frequency range between 1.5–3.3 Hz, indicating the fast-varying temporal structures at a timescale of 0.3–0.7 s. This is the same timescale previously reported in the observations of HXR fast variations (Kiplinger et al. 1983; Kiplinger et al. 1984; Kiplinger, Dennis, & Orwig 1989; Neidig et al. 1993).

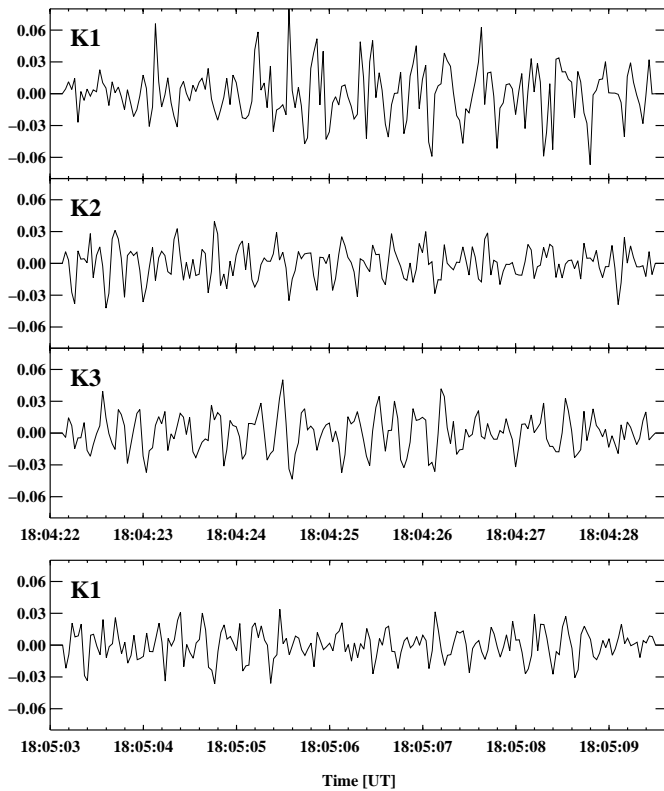


FIG. 7.—Time profiles of  $H\alpha-1.3 \text{ \AA}$  flare emission. The 10-point smoothed background is subtracted from all the curves. The top three panels show fluctuations at three flare kernels in the time interval shown in Fig. 5. The bottom panel shows the variations at K1 in a time interval 40 s later.

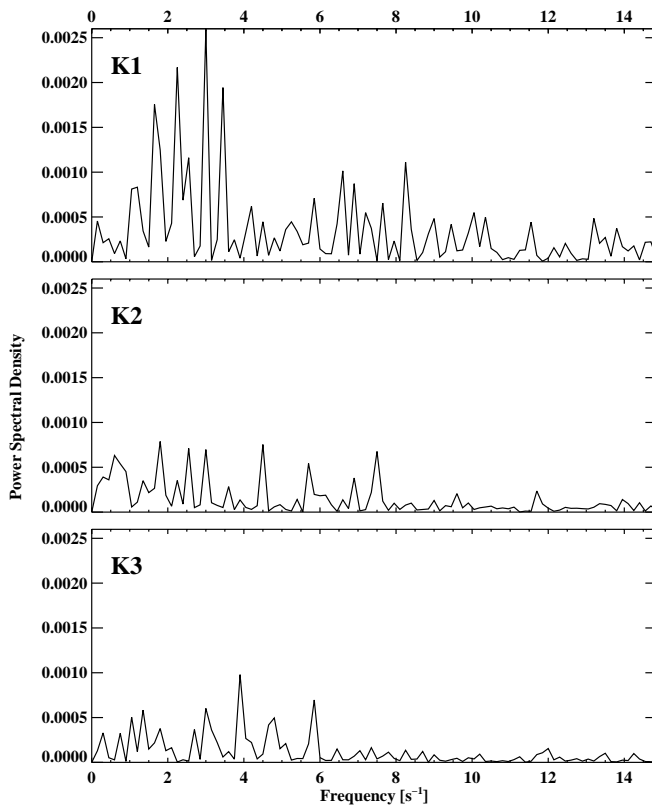
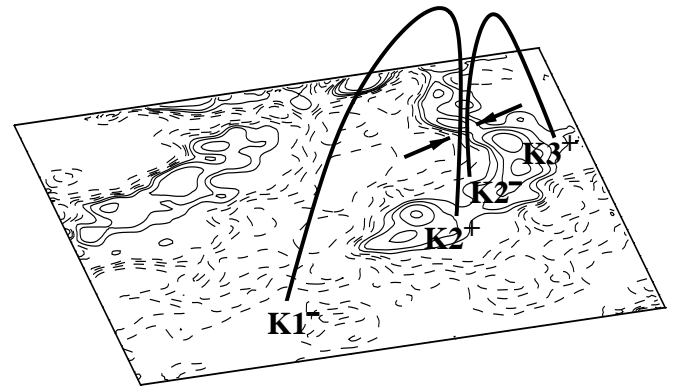


FIG. 8.—Power spectra of the fast variations of the  $H\alpha-1.3 \text{ \AA}$  emission at the three flare kernels 18:04:22–18:04:29 UT.

(a) Before reconnection



(b) After reconnection

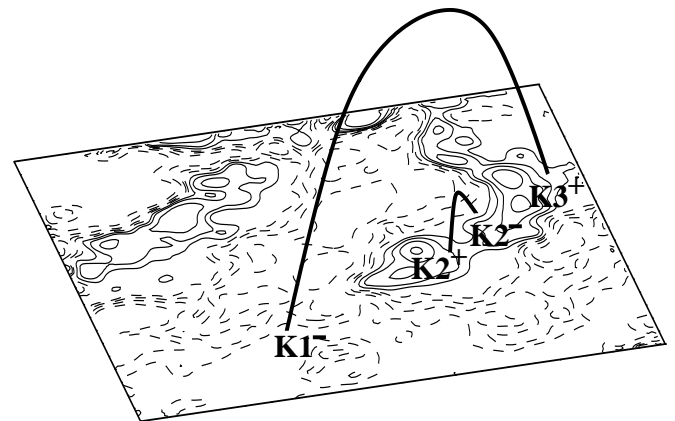


FIG. 9.—Sketch of the magnetic configuration of the flare before and after the reconnection. The background contours show the line-of-sight magnetogram taken before the flare as in Fig. 3. The solid (dashed) lines indicate the positive (negative) magnetic polarities, and the contour levels are  $\pm 20, 50, 100, 200 \text{ G}$ .

Note that such high-frequency fluctuations only exist in this time interval, when the best temporal correlation between  $H\alpha-1.3 \text{ \AA}$  and HXR emission is present. In the bottom panel of Figure 7, we also plot a similar curve for K1 at a different time interval 40 s later, when there is no HXR emission. The amplitude of fluctuation in this panel is comparable to that in the second panel. Such comparison indicates that the high-frequency fluctuations observed at K1 during the 18:40 UT time interval were related to the so-called “elementary HXR burst.”

From the original images, we examine K1 carefully. The fluctuations reflect intensity changes in the same patches at a spatial scale of less than  $1''$ , but not appearances/disappearances of different small patches. With even higher spatial resolution, the fast fluctuations may be fully spatially resolved.

We admit that the origin of the rapid fluctuations in kernel K1 is still unclear when there is no high-cadence hard X-ray to compare with. We cannot rule out the possibility that the fluctuation in K1 is due to seeing,

However, we believe that we tried everything that we could test for this specific case, and found no evidence that the larger fluctuation is due to the seeing. We have also tried different boxes covering kernels when we calculated the fluxes and found no difference in the time profiles. So selection of the box is not a problem. Images are destretched; differential seeing is very small. The absolute confidence will only come out of the comparison with hard X-ray time profile. Until HESSI is operational, we probably will not be able to have absolute claim on this point for similar observations.

### 3.5. Summary of Results

We analyzed high-cadence observations of a C5.7 flare on 1999 August 23 and obtained the following results:

1. Three flare kernels were observed in  $H\alpha - 1.3 \text{ \AA}$  during the impulsive phase of the flare. The flare starts in a non-magnetic area at the magnetic neutral line. We developed a scenario that the top of a dense low-lying loop is the initial energy release site.

2. We analyzed the temporal behavior of these three kernels with respect to the HXR emission. We find that during a 7 s period, the brightening at one of the three flare kernels (K1), possibly the footpoint of a flare loop, follows the variation of the HXR flux very well. Therefore, we conclude that it is the source of HXR emission.

3. The flare kernel K1 illustrates best the correlation with HXR. The  $H\alpha$  emission at this kernel shows fast fluctuation at a timescale of 0.3–0.7 s. They are the real signature of temporal fine structure of the flare, and they indicate high-frequency electron acceleration and precipitation at the footpoint of the flare loop, which also gives rise to the HXR “elementary bursts” as reported by Kiplinger, Dennis, & Orwig (1989).

The three observed flare kernels at  $H\alpha - 1.3 \text{ \AA}$  are located at the top of a compact loop, and two footpoints of a long, overlying loop. The low-lying compact loop is the product of magnetic reconnection (see Fig. 9), while the HXR-correlated footpoint brightenings demonstrate high-frequency variations which are an important impulsive phase behavior of solar flares.

## 4. DISCUSSIONS

Our high-cadence observations are designed to investigate the “elementary bursts” previously reported in the HXR and radio microwave observations. From the above analysis, we have obtained positive evidence that the variations in the HXR burst and  $H\alpha - 1.3 \text{ \AA}$  emission are strongly correlated, and we may have confirmed the existence of high-frequency variation from our  $H\alpha$  observations. Our observations demonstrate that the dominant fast variations in the impulsive phase of the flare are on a timescale of 0.3–0.7 s, which can be unambiguously detected with a temporal resolution of better than 0.066 s. The subsecond HXR bursts are supposed to represent “quantized” injections of accelerated electrons (Benz et al. 1994), possibly as the result of many small-scale reconnections (Vlahos 1989). The fact

that we have not observed changes of the locations of the impulsive  $H\alpha - 1.3 \text{ \AA}$  emission sources suggests that the filamentary structures are confined to a scale of less than a few hundred kilometers at the level of photosphere.

The chromospheric observations were made at  $H\alpha$  blue wing based on the assumption that the  $H\alpha$  blue wing emission should come from a “thick-target” via Stark broadening by nonthermal electrons penetrating into the deep chromosphere. Out of the three flare kernels studied, two can be identified as deep chromospheric footpoint sources, but we also discover a possible loop top source that is apparently not located at a magnetic element but at the magnetic neutral line. It raises the interesting question: what kind of chromospheric heating mechanism can produce  $H\alpha - 1.3 \text{ \AA}$  emission at the top of a loop? Since the most important condition to produce  $H\alpha$  far wing emission is the electron density, this loop must be very low and dense. If the magnetic reconnection occurs at a low altitude in this loop, it is also likely that after the impulsive phase when HXR emission ends, heating of the chromosphere via thermal conduction in the flare loop could be very efficient, and  $H\alpha - 1.3 \text{ \AA}$  is probably still not far enough from the line center to avoid thermal impact.

It is also puzzling that the HXR emission peaks at least 2–3 s before the  $H\alpha - 1.3 \text{ \AA}$  emission in the very early stage of the impulsive phase. This nonnegligible delay of chromospheric off-band emission with respect to the HXR emission may be due to the ionization timescale of the chromosphere. According to Canfield & Gayley (1987), the chromospheric ionization timescale is determined by the intensity of the nonthermal flux deposited to the chromosphere. For the nonthermal flux of  $1 \times 10^{11} \text{ ergs cm}^{-2} \text{ s}^{-1}$ , this timescale is estimated to be 0.3–0.4 s, while for less strong flux, the ionization timescale can amount to a few seconds; hence, the delay of  $H\alpha$  emission can be as large as a few seconds. Since the flare is only a C5.7 event, the HXR flux is at least 1 order of magnitude weaker than  $1 \times 10^{11} \text{ ergs cm}^{-2} \text{ s}^{-1}$ . We propose that the observed time delay in the early impulsive phase is due to ionization of the cool chromosphere. While 30 s later, we observe a good temporal correlation between hard X-ray bursts and  $H\alpha$  emission, because by then, the chromosphere is sufficiently ionized and can respond promptly to the further input of electron beams which also produce HXR bursts in the late impulsive phase. It is unlikely that the time delay in the early stage is thermal in nature. According to Abbett & Hawley (1999), in the presence of nonthermal beams, as evidenced by HXR emission, the thermal influence on the chromosphere is negligible.

We are grateful to the observing staff at BBSO for their support in obtaining the data. We thank D. E. Gary, V. B. Yurchyshyn, J. Chae, and M. Ding for reading the manuscript and helpful discussion. The work is supported by NSF under grants ATM-0076602, ATM-9714796 and ATM-9713359, NASA under grants NAG5-9501, NAG5-7350 and NAG5-7085, and ONR under grant N00014-97-1-1037.

## REFERENCES

- Abbott, W. P., & Hawley, S. L. 1999, *ApJ*, 521, 906
- Aschwanden, M. J., Wills, M. J., Hudson, H. S., Kosugi, T., & Schwartz, R. A. 1996, *ApJ*, 468, 398
- Benz, A. O., Kosugi, T., Aschwanden, M. J., Benka, S. G., Chupp, E. L., Enome, S., Garcia, H., Holman, G. D., Kurt, V. G., Sakao, T., Stepanov, A. V., & Volwerk, M. 1994, *Sol. Phys.*, 153, 33
- Brown, J. 1971, *Sol. Phys.*, 18, 489
- Canfield, R. C., & Gayley, K. G. 1987, *ApJ*, 322, 999
- Canfield, R. C., Gunkler, T. A., & Ricchiazzi, P. J. 1984, *ApJ*, 282, 296
- de La Beaujardiere, J.-F., Kiplinger, A. L., & Canfield, R. C. 1992, *ApJ*, 401, 761
- Denker, C., Johannesson, A., Marquette, W. H., Goode, P. R., Wang, H., & Zirin, H. 1999, *Sol. Phys.*, 184, 87
- Emslie, A. J. 1978, *ApJ*, 224, 241
- Fang C., Henoux, J. C., & Gan W. 1993, *A&A*, 274, 917
- Fisher, G. H., Canfield, R. C., & McClymont, A. N. 1985, *ApJ*, 289, 425
- Goode, P. R., Wang, H., Marquette, W. H., & Denker, C. 2000, *Sol. Phys.*, in press
- Hawley, S. L., & Fisher, G. H. 1994, *ApJ*, 426, 387
- Kaempfer, N., & Magun, A. 1983, *ApJ*, 274, 910
- Kiplinger, A. L., Dennis, B. R., Emslie, A. G., Frost, K. L., & Orwig, L. E. 1983, *ApJ*, 265, L99
- Kiplinger, A. L., Dennis, B. R., Frost, K. L., & Orwig, L. E. 1984, *ApJ*, 287, L105
- Kiplinger, A. L., Dennis, B. R., & Orwig, L. E. 1989, in *Proc. Max'91 Workshop*, ed. R. M. Winglee & B. R. Dennis (Greenbelt: NASA), 346
- Lin, R. P., et al. 1998, *Proc. SPIE*, 3442, 2
- Neidig, D. F., Kiplinger, A. L., Cohl, H. S., & Wiborg, P. H. 1993, *ApJ*, 406, 306
- Sturrock, P. A. 1989, in *Proc. Max'91 Workshop*, ed. R. M. Winglee & B. R. Dennis (Greenbelt: NASA), 1
- Svestka, Z. 1976, *Solar Flares* (Dordrecht: Reidel)
- Varsik, J. R. 1995, *Sol. Phys.*, 161, 207
- Vlahos, L. 1989, *Sol. Phys.*, 121, 431
- Wulser, J. P. & Marti, H. 1989, *ApJ*, 341, 1088